



Large-scale emission from Fanaroff-Riley galaxies

P. Bordas^{1,2}

¹ Institut für Astronomie und Astrophysik, Universität Tübingen, Sand 1, 72076 Tübingen, Germany, e-mail: pol.bordas@uni-tuebingen.de

² *INTEGRAL* Science Data Centre, Université de Genève, Chemin d'Ecogia 16, CH-1290 Versoix, Switzerland

Abstract. The termination structures of the jets of Fanaroff & Riley galaxies are observed to produce extended non-thermal emission in a wide frequency range. The study of these structures can provide valuable insights on the conditions for particle acceleration and radiation at the front shocks. In this work we focus on the emission seen from FRI sources. The *Fermi* Collaboration has recently reported the detection of high-energy gamma-rays from Cen A lobes. This is the first time that gamma-rays are observed from the interaction regions of this kind of sources. Making use of a radiative code based on the results of relativistic numerical simulations of the evolution of a FRI jet, we make predictions for the spectra and lightcurves of the thermal and non-thermal emission at different stages of evolution of FRI sources. The relative importance of the thermal and non-thermal emission as a function of the source age is discussed, as well as the synchrotron to Inverse Compton (IC) balance in the resulting source spectra. The energy-dependent extended morphology is also briefly discussed, the main results being the compactness of the hard X-ray and putative TeV emission as compared to the more extended radio and GeV emission. non-thermal broadband emission from the termination regions of FRI jets could be detectable for sources located up to distances of a few 100 Mpc.

Key words. galaxies: evolution—galaxies: jets—galaxies: kinematics and dynamics—X-rays: galaxies—gamma-rays: galaxies—radio continuum: galaxies

1. Introduction

Fanaroff-Riley sources of type I and II (FRI-II, Fanaroff & Riley 1974) are radio loud Active Galactic Nuclei (AGN) displaying large-scale jets that interact with the surrounding ISM/ICM medium. The phenomenological division between FRI and FR II is based on the much longer length-scales of the collimated jet in the latter, probably due to its intrinsically higher carried power. The rela-

tivistic jets in FRI galaxies are disrupted in shorter distances than in FR IIs, that can propagate further away and produce radio lobes and non-thermal emitting hot spots. The study of the extended emission in FRI/II sources can be used to derive the properties of the flows and the surrounding medium. In this regard, Heinz, Reynolds & Begelman (1998) used a simple evolutionary model to conclude that only for dense enough media the extended X-ray emission could be expected even for powerful FR II jets. At higher energies, Kino, Kawakatu & Ito (2007) estimate that the ther-

mal MeV radiation from cocoons of radio galaxies is significant only for sources with ages $\ll 10^7$ yrs. Furthermore, non-thermal X-ray synchrotron and/or IC emission has been observed in several sources (see e.g. Kataoka et al. (2003); (Croston et al. 2009); (?)). Recently, the detection by *Fermi* of extended GeV emission in the radio lobes of Cen A (Abdo et al. 2010), show that acceleration up to VHE is taking place in the disrupted jet region. Numerical simulations, on the other hand, have demonstrated to be a powerful tool to further study the jet/medium interactions. Perucho & Martí (2007) performed a simulation aimed to test the FRI jet evolution paradigm (Bicknell 1984). We computed the thermal and non-thermal emission from FRI sources obtained with a radiative model adapted from (Bordas et al. 2009) that takes as input the results of those simulations to characterize the conditions of the shocked regions. Below, we discuss the numerical simulations, the radiation model used. We then discuss the obtained results and the relevance of the thermal and non-thermal radiation at different energy bands. For a more extended discussion, the reader is referred to Perucho & Martí (2007) and Bordas et al. (2011).

2. Hydrodynamical simulations and radiation model

The numerical simulations of Perucho & Martí (2007) have been used to characterize the physical properties of the jet/medium shocked regions. The jet is injected in the numerical grid at 500 pc from the active nucleus, with a radius of 60 pc. The ambient medium, composed by neutral hydrogen, has a profile in pressure (see e.g. Hardcastle et al. 2002). The jet, leptonic in composition, has an initial velocity $v_{j0} = 0.87c$, a density ratio with respect to the ambient $\rho_{j0}/\rho_{a0} = 10^{-5}$, a pressure ratio with the ambient $P_{j0}/P_{a0} \simeq 8$, and temperature 4×10^9 K, resulting in a kinetic luminosity $L_j = 10^{44}$ erg s $^{-1}$. Further details on the simulation code can be found in Perucho & Martí (2007). Regarding the radiative code, we used a simplified one-zone model to study the emission properties of both shell and co-

coon regions. The injected non-thermal luminosity is = 10% of the total jet kinetic luminosity L_j . The magnetic field B has been fixed taking the magnetic energy density to be 10% of the ram/thermal pressure. Concerning particle acceleration, the recollimation shock is assumed to be the accelerator of particles in the cocoon region. We use a relativistic approach in this case, with an acceleration rate $\dot{E} = \eta q B c$ with $\eta = 0.1$. For the bow shock, we have adopted instead a non-relativistic approach in view of the lower shock velocities $\sim (1 - 2) \times 10^8$ cm s $^{-1}$. The particle energy distribution at a given time, $N(E, t_{\text{src}})$, is calculated considering the injection ($\propto E^{-p}$, with $p = 2.1$), at any time t_{src} . Maximum particle energies, $E_{\text{max}}(t)$, vary also along time, through the magnetic field, the accelerator size and the shock velocity dependence. Further details on the radiative code can be found in Bordas et al. (2009) and Bordas et al. (2011).

3. Results

Non-thermal emission. The non-thermal spectral energy distributions (SED) for the cocoon and the shell, at $t_{\text{src}} = 10^5$, 3×10^6 and 10^8 yr, are shown the left and center panels of Fig. 1. The obtained radio and X-ray synchrotron luminosities in both regions are at the level of 2×10^{41} erg s $^{-1}$. The approximate constancy of the luminosities with time is due to the fact that particles have reached the steady state at t_{src} through synchrotron cooling and the assumed constancy of L_{nt} . The decrease of B with time, and therefore the growth of t_{syn} , is compensated by the increase of time available for cooling. The IC luminosity grows as long as this process becomes more efficient compared to synchrotron and adiabatic cooling, which is shown by the decrease of u_B/u_{rad} from $\approx 5 \times 10^3$ (10^5 yr) to 4 (10^8 yr). The cocoon and the shell have similar HE luminosities, but the cocoon is few times brighter at VHE than the shell due the higher maximum energies that particles can attain in the former. In both regions the bolometric IC luminosities grow similarly with time, reaching $\sim 10^{42}$ and 10^{41} erg s $^{-1}$ at HE and VHE, respectively. The lightcurves for

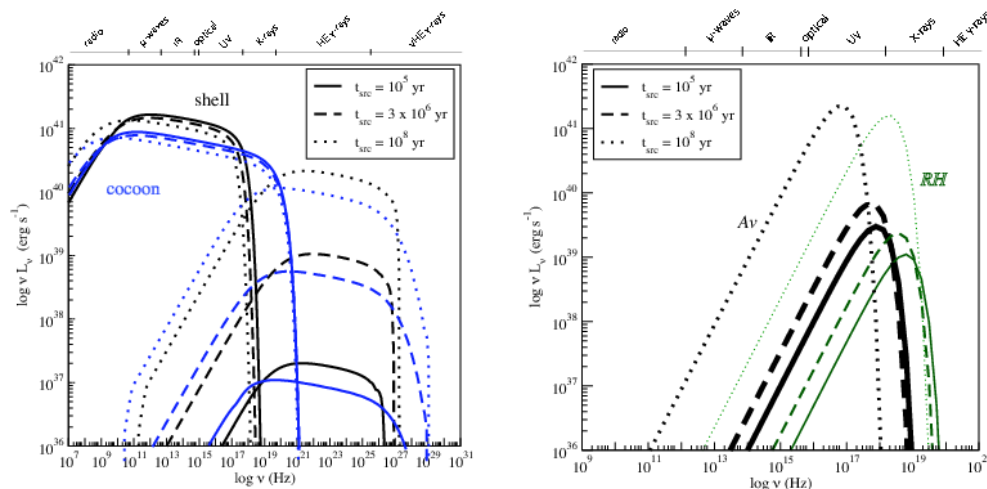


Fig. 1. Computed SEDs of the synchrotron, IC as well as Bremsstrahlung emission for three different ages: 10^5 (solid line), 3×10^6 (long-dashed line) and 10^8 yr (dotted line). Both shell and cocoon contribute to the overall non-thermal emission, whilst only the shell is considered for the thermal emission, which has been splitted into two components: one corresponding to the average shell properties (A_v , black), and another one related to a shell region with conditions similar to those of Rankine-Hugoniot (RH , green). The SEDs account for the contribution of one jet/medium interaction region only, so the values here should be scaled by a factor of two to get the whole source emission.

the luminosities in radio (at 5 GHz), X-rays (1–10 keV), HE (0.1–100 GeV) and VHE (0.1–100 TeV), for the cocoon and the shell, are presented in Fig. 2. They show in more detail the time behavior of the non-thermal radiation at different wavelengths discussed above. The complex and smooth shape of the lightcurves, most clear for the HE and the VHE emission, is a consequence of the hydrodynamical evolution of the whole interaction structure propagating in an inhomogeneous external medium.

Thermal emission. Thermal emission has been considered only for the shell, much denser than the cocoon. Furthermore, we have simplified the calculations considering two separate regions: one, cooler (ultraviolet -UV/soft X-rays) but brighter, corresponds to the averaged shell conditions (A_v), and another one, fainter but hotter (hard X-rays), corresponds to a region close to the apex of the bow shock (RH), in which the shell has properties close to those given by the jump conditions of Rankine-Hugoniot. The volume of the latter region is about 3 – 4% of that of

the whole shell. Figure 1, right panel, shows the thermal SEDs for $t_{\text{src}} = 10^5$, 3×10^6 and 10^8 yr. The slowdown of the bow shock and the velocity dependence of the postshock temperature, $\propto v_{\text{bs}}^2$, leads to a decrease in the peak of the thermal emission with time. The overall luminosity increase however as the source gets older, from 10^{39} to few times 10^{41} erg s^{-1} , since the Bremsstrahlung time-scale is $t_{\text{Brems}} \approx 10^3 T^{1/2} n_e^{-1} \approx 5 \times 10^9$ yr $\gg t_{\text{src}}$, with the shell and the hot postshock region components peaking from soft X-rays to UV and from hard to soft X-rays, respectively. Thermal Bremsstrahlung increases from $t_{\text{src}} = 10^5$ to $\sim 10^6$ yr, then the luminosity slightly decreases until $t_{\text{src}} \sim 3 \times 10^6$ yr, when a transition in the external medium from the denser galaxy core to the rarefied galaxy group medium is produced, and increases again afterwards. The component A_v dominates the thermal bolometric luminosity in young sources, but the component RH becomes similarly bright at $t_{\text{src}} \sim 10^8$ yr.

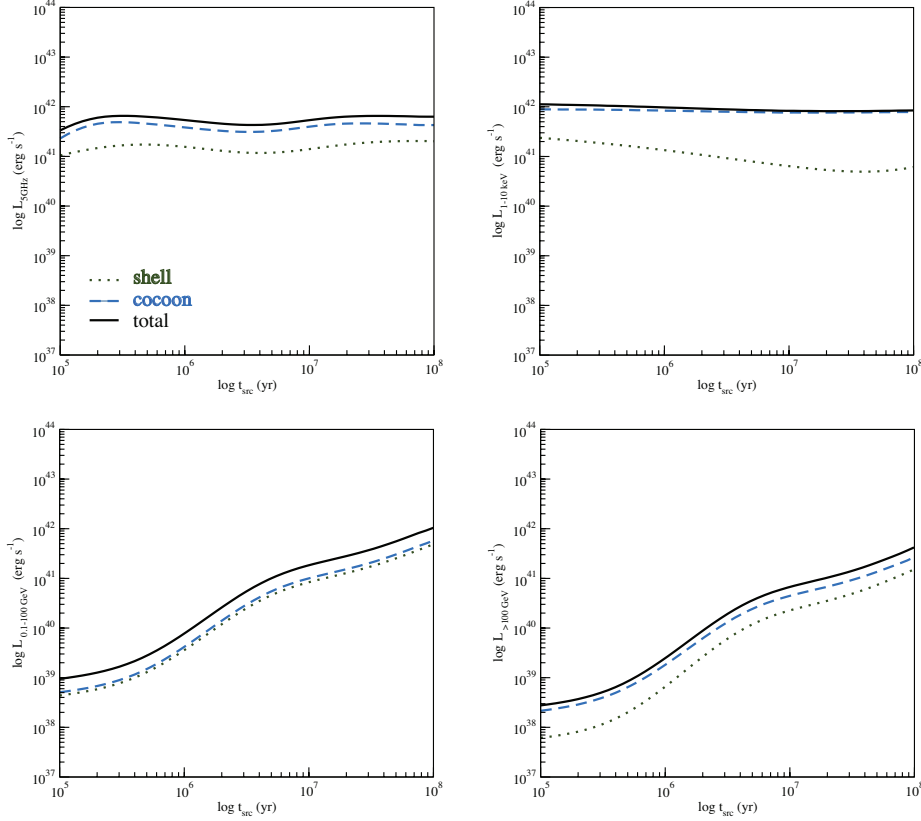


Fig. 2. Computed non-thermal lightcurves of the radio (5 GHz $\times L_5$ GHz, top-left), X-ray (bolometric: 1–10 keV, top-right) and gamma-ray emission (bolometric: 0.1–100 GeV, bottom-left; bolometric: > 100 GeV: bottom-right) in the age range $t_{\text{src}} = 10^5 - 10^8$ yr.

4. Discussion

Our results can be discussed on the ground of the thermal and non-thermal fluxes predicted at different energy bands. In radio, the cocoon dominates with fluxes up to $\sim 10^{-12} (d/100 \text{ Mpc})^{-2} \text{ erg cm}^{-2} \text{ s}^{-1} \sim 10 \text{ Jy}$ at 5 GHz from a region of few times $10' (d/100 \text{ Mpc})^{-1}$ of angular size. The flux level is comparable to those observed for instance in 3C 31 and 3c 15, with radio luminosities at 4.75 GHz of about $3 \times 10^{40} \text{ erg/s}$ (Andernach et al. 1992), and $F_{\text{radio}} \sim 10^{-14} \text{ erg cm}^{-2} \text{ s}^{-1}$ ($d \sim 300 \text{ Mpc}$) (Kataoka et al. 2003), respectively. The shell radio flux is slightly below the cocoon one, although limb brightening may enhance the detectability of

the former. The radio lightcurve is quite steady, since the accumulation of electrons compensates the weakening of the magnetic field with t_{src} . We note that given the moderate velocities of the bow shock, thermal photons cannot reach energies as high as those discussed in Kino, Kawakatu & Ito (2007).

At X-rays, the different thermal emitting regions in the shell would lead to a bolometric flux from $\sim 10^{-15} (d/100 \text{ Mpc})^{-2}$ (10^5 yr) to few times $10^{-13} (d/100 \text{ Mpc})^{-2} \text{ erg cm}^{-2} \text{ s}^{-1}$ (10^8 yr). The hard X-rays would be located at the apex of the bow shock, with typical angular size of a few $1' (d/100 \text{ Mpc})^{-1}$ (for $t_{\text{src}} \sim 10^8$ yr), whilst lower energy X-rays would come from the whole shell, with of a few $10' (d/100 \text{ Mpc})^{-1}$.

Regarding non-thermal X-rays, the cocoon dominates the total output, with fluxes $\sim 10^{-13} (d/100 \text{ Mpc})^{-2} \text{ erg cm}^{-2} \text{ s}^{-1}$, although limb brightening effects may again increase the shell flux. In fact, in the case of Cen A, the shell seems to be the dominant source of non-thermal X-rays Croston et al. (2009). This difference could be explained by a higher E_{max} in the shell of that source. The non-thermal X-ray fluxes $\sim 10^{-14} \text{ erg cm}^{-2} \text{ s}^{-1}$ of 3C 15 reported by Kataoka et al. (2003) imply a non-thermal luminosity of $\approx 1.3 \times 10^{41} \text{ erg s}^{-1}$ at 300 Mpc, in good agreement with the values predicted here. Furthermore, synchrotron emission concentrated around the recollimation shock is compatible with the large-scale jet X-ray emission found in 3C 31 by Hardcastle et al. (2002). If a strong recollimation shock is indeed the origin of these large-scale jet X-rays, then the hypothesis that jet disruption in 3C 31 is caused by shock triggered instabilities is favored against stellar wind mass-load (Laing & Bridle 2002). Finally, we note that for sources older than those considered here and/or lower B -values, the synchrotron emission would be less relevant and IC would dominate the X-ray output.

The SEDs in the HE-VHE range are similar for both the cocoon and the shell. The HE SED is close to flat, and becomes steeper at VHE. We have not accounted for EBL gamma-ray absorption, which would become significant at distances larger than 100 Mpc. The overall emission increases with time mainly due to the increasing efficiency of the CMB IC channel as compared with synchrotron and adiabatic losses. Gamma-ray fluxes for a source with $t_{\text{src}} \sim 10^8 \text{ yr}$ are around $\sim 10^{-12} (d/100 \text{ Mpc}) \text{ erg cm}^{-2} \text{ s}^{-1}$. At HE, such a source may require very long exposures to be detected by, e.g., *Fermi*, unless it is very nearby (e.g. Cen A, Abdo et al. 2010) or shows a higher non-thermal efficiencies and/or jet power. At VHE, the fluxes could be observed by the current IACTs, although the extension of the source, of tens of arcminute at 100 Mpc, and the steep spectrum above $\sim 100 \text{ GeV}$, may make a detection possible only after a long. The forthcoming CTA may however allow the

detection of VHE emission from FRI jet lobes, and possibly carry out energy-dependent morphological studies.

From our study we conclude that, for moderate non-thermal luminosities, radio lobes of FRI radio galaxies are good candidates to be detected in the whole spectral range, with the radiation appearing extended in most of the energy bands. Soft X-rays will be likely dominated by synchrotron emission up to ages $\sim 10^8 \text{ yr}$, with IC tending to be dominant for older sources. Thermal X-rays seem unavoidable and may dominate in hard X-rays in old sources even if a non-thermal component is present. The low surface brightness may require long observation times for the detection in X- and gamma-rays, although the steady nature of these sources can help in this regard.

Acknowledgements. PB acknowledges the close collaboration with V. Bosch-Ramon and M. Perucho. PB acknowledges support from the German Federal Ministry of Economics and Technology through DLR grant 50 OG 1001. PB also acknowledges the excellent work conditions at the *INTEGRAL* Science Data Center.

References

- Fanaroff B.L. & Riley J.M., 1974, MNRAS, 167, 31
 Abdo, A. A. et al. 2010a, Science, 328, 725
 Heinz S., Reynolds C. S., Begelman M. C., 1998, ApJ, 501, 126
 Kino M., Kawakatu N., Ito H., 2007, MNRAS, 376, 1630
 Kataoka, J., et al. 2003, A&A, 410, 833
 Croston J. H., et al., 2009, MNRAS, 395, 1999
 Perucho M., Martí J. M., 2007, MNRAS, 382, 526 (PM07)
 Bicknell G. V., 1984, ApJ, 286, 68
 Bordas P., Bosch-Ramon V., Paredes J. M., Perucho M., 2009,
 Bordas, P., Bosch-Ramon, V. & Perucho, M. 2011, MNRAS, 412, 1229
 Andernach, H., et al. 1992, A&AS, 93, 331
 Hardcastle M. J., et al. 2002, MNRAS, 334, 182
 Laing R. A., Bridle A. H., 2002, MNRAS, 336, 1161